CFL Number Insensitive CESE Schemes For the Two-Dimensional Euler Equations

Moujin Zhang[1], S.-T. John Yu[2]
Mechanical Engineering Department
Wayne State University, Detroit, MI 48202

Sin-Chung Chang[3]
NASA Glenn Research Center
Cleveland, OH 44135

Abstract

The CESE method is a new numerical method for nonlinear hyperbolic conservation laws. The method is explicit, and the stability bound is CFL number <1.0. The method can provide time accurate solution of unsteady flows with complex shock structure. However, the CESE method may become overly dissipative for small CFL numbers. Recently, Chang [9] proposed new CFL insensitive CESE schemes for the Euler equations in one spatial dimension. The new scheme could crisply resolve shock and contact discontinuity for CFL numbers less than 0.001. In the present paper, we extend Chang's new schemes for the Euler equations in two spatial dimensions. Numerical results of reflected oblique shocks show that the new CESE schemes can resolve shocks crisply for a wide range of CFL numbers.

1. Introduction

The space-time conservation element and solution element (CESE) method is a novel CFD method for hyperbolic conservation laws. Contrast to modern upwind schemes, no Riemann solver and/or reconstruction procedure are used as the building blocks, and the logic and the operation count of the CESE method are much simpler and more efficient. Nevertheless, the CESE method is superb for resolving complex shock systems and shock/acoustics interactions. Numerous results have been obtained by using the CESE method [1-8], including flows with steady and moving shock waves, acoustic waves, flows dominated by vortices, detonations, dam-break flows with hydraulic jump, cavitations, turbulent flows with embedded sprays, and magneto-hydrodynamics.

However, numerical dissipation of the original CESE schemes tends to increase with decreasing CFL number. In particular, when CFL numbers are less than 0.1, the artificial damping becomes visibly detrimental to the fine flow structures. Because CFL numbers may vary significantly in the computational domain due to non-uniform mesh, the solution may become too dissipated in certain region. To overcome this problem, Chang [9] proposed the CFL number insensitive schemes for the Euler equations in one spatial dimension. Numerical results of the Sod shock tube problem showed that the for 0.001 < CFL < 1, Chang's new method could crisply resolve the shock wave and the contact discontinuity.

The present paper is an extension of Chang's CFL number insensitive schemes for equations in two spatial dimensions. The rest of paper is organized as follows. In Section 2, we review the two-dimensional CESE method. In section 3, we illustrate the CFL condition in two spatial domain in the setting of the CESE method. In section 4, we illustrate the new CFL number insensitive schemes in two spatial dimensions. Section 5 shows the numerical result of reflected oblique shock wave for a wide range of the CFL numbers. We then offer concluding remarks and provide cited references.

[1] Research Associate, mzhang@eng.wayne.edu
[2] Associate Professor, styu@eng.wayne.edu
[3] Aerospace Engineer, Email: sin-chung.chang@lerc.nasa.gov

2. The 2D CESE Method

2.1 Space-Time Integration

The Euler equations in two-spatial-dimensions can be expressed as

$$\frac{\partial u_m}{\partial t}+\frac{\partial f_m}{\partial x}+\frac{\partial g_m}{\partial y}=0\,, \tag{2.1}$$

for m = 1, 2, 3, 4, where u_m, f_m and g_m are flow variables, and fluxes in x- and y-directions, respectively, and they are defined as

$$\begin{pmatrix} u_1 \\ u_2 \\ u_3 \\ u_4 \end{pmatrix}=\begin{pmatrix} \rho \\ \rho u \\ \rho v \\ e \end{pmatrix}, \tag{2.2a}$$

$$\begin{pmatrix} f_1 \\ f_2 \\ f_3 \\ f_4 \end{pmatrix}=\begin{pmatrix} \rho u \\ \rho u^2+p \\ \rho uv \\ (e+p)u \end{pmatrix} \tag{2.2b}$$

$$\begin{pmatrix} g_1 \\ g_2 \\ g_3 \\ g_4 \end{pmatrix}=\begin{pmatrix} \rho v \\ \rho vu \\ \rho v^2+p \\ (e+p)v \end{pmatrix}. \tag{2.2c}$$

where ρ, p, u and v are density, pressure, and velocity components in x- and y-direction. The specific total energy

$$e=p/(\gamma-1)+\rho\left(u^2+v^2\right)/2\,,$$

where $\gamma = 1.4$ is the specific heat ratio. To proceed, let $x_1=x$, $x_2=y$ and $x_3=t$ be the coordinates of a three-dimensional Euclidean space E_3. Equation (2.1) becomes the divergence free condition in E_3,

$$\nabla\cdot\mathbf{h}_m=0\,, \tag{2.3}$$

where $\mathbf{h}_m=(f_m,g_m,u_m)$ is the current density vector. By Gauss' divergence theorem,

$$\int_V \nabla\cdot\mathbf{h}_m dV=\oint_{S(V)}\mathbf{h}_m\cdot d\mathbf{s}=0\,, \tag{2.4}$$

for m = 1, 2, 3, 4, where *S(V)* is the boundary of an arbitrary space-time region V in E_3 and $d\mathbf{s}=\mathbf{n}d\sigma$, where $d\sigma$ and $\mathbf{n}$ are the area and the outward unit normal vector of a surface element on *S(V).*

2.2 Discretization by CE and SE

The two-dimensional spatial domain is divided into no-overlapped triangles. Refer to Fig. 1. Point G, the centroid of ΔBDF, is marked by a solid circle, and A, C and E, centorids of ΔFMB, ΔBJD and ΔDLF, and are marked by hollow circles. In Fig. 2, A, B, C, D, E and F form a hexagon ABCDEF. Point $\overline{G}$, marked by a solid square is the centroid of hexagon ABCDEF, and it is the solution point of ΔBDF. Let S_{q1}, S_{q2} and S_{q3} be areas of quadrilaterals ABGF, BCDG and DEFG, and (x_{q1},y_{q1}), (x_{q2},y_{q2}) and (x_{q3},y_{q3}) be the spatial coordinates of their centroids. The spatial coordinates of point $\overline{G}$ are

$$\begin{aligned} x_{\overline{G}}&=\frac{S_{q1}x_{q1}+S_{q2}x_{q2}+S_{q3}x_{q3}}{S_{q1}+S_{q2}+S_{q3}} \\ y_{\overline{G}}&=\frac{S_{q1}y_{q1}+S_{q2}y_{q2}+S_{q3}y_{q3}}{S_{q1}+S_{q2}+S_{q3}} \end{aligned}. \tag{2.5}$$

Points $\overline{A}$, $\overline{C}$ and $\overline{E}$, marked by hollow squares in Fig. 2, and are the solution points of ΔFMB, ΔBJD and ΔDLF, respectively. In the space-time domain, A, B, C, D, E, F and G are at the time level $n-1/2$, and A' B', C', D', E', F' and G' are at the time level n. Points A'', B'', C'', D'', E'', F'' and G'' are at the time level $n+1/2$. Let j, k and n be indices for x, y and t, respectively. Points G', A, C and G are marked by (j,k,n) , $(j1,k1,n-1/2)$, $(j2,k2,n-1/2)$ and $(j3,k3,n-1/2)$, respectively. Shown in Fig. 1c, the solution points $\overline{G}'$, $\overline{A}$, $\overline{C}$ and $\overline{E}$ are placed in a staggered positions in E_3, and their coordinates are (j,k,n) , $(j1,k1,n-1/2)$, $(j2,k2,n-1/2)$ and $(j3,k3,n-1/2)$. Note that, a triangle's centroid G' and the associated solution point, $\overline{G}'$ have different spatial coordinates. In the calculation, flow variables are stored at the solution points.

As presented in Fig. 4, the solution element $SE(j,k,n)$ associated with point G' (j,k,n), is the union of four planes, i.e., the hexagon $A'B'C'D'E'F'$, the quadrilaterals $B''BGG''$, $D''DGG''$ and $F''FGG''$, and their intermediate neighborhood. Similarly, there are three SEs, i.e., $SE(j1,k1,n-1/2)$, $SE(j2,k2,n-1/2)$ and $SE(j3,k3,n-1/2)$ associated with points A, C and E, respectively. The surfaces of the four SEs form three CEs for point G'. Refer to Fig. 3. Three CEs are quadrilateral cylinders $ABGFA'B'G'F'$, $CDGBC'D'G'B'$ and $EFGDE'F'G'D'$, and are referred to as $CE_1(j,k,n)$, $CE_2(j,k,n)$ and $CE_3(j,k,n)$, respectively. $CE(j,k,n)$ is the union of $CE_1(j,k,n)$, $CE_2(j,k,n)$ and $CE_3(j,k,n)$.

Inside $SE(j,k,n)$, the first-order Taylor series expansion is employed to descritize the flow variables and fluxes:

$$u_m^*(x,y,t;j,k,n) = (g_m)_{j,k}^n + (g_{mx})_{j,k}^n (x - x_{j,k}) + (g_{my})_{j,k}^n (y - y_{j,k}) + (g_{mt})_{j,k}^n (t - t^n), \quad (2.6)$$

$$f_m^*(x,y,t;j,k,n) = (g_m)_{j,k}^n + (g_{mx})_{j,k}^n (x - x_{j,k}) + (g_{my})_{j,k}^n (y - y_{j,k}) + (g_{mt})_{j,k}^n (t - t^n), \quad (2.7)$$

$$g_m^*(x,y,t;j,k,n) = (g_m)_{j,k}^n + (g_{mx})_{j,k}^n (x - x_{j,k}) + (g_{my})_{j,k}^n (y - y_{j,k}) + (g_{mt})_{j,k}^n (t - t^n), \quad (2.8)$$

for m = 1, 2, 3, 4. In Eqs. (2.6-8), $(u_m)_{j,k}^n$, $(u_{mx})_{j,k}^n$ and $(u_{my})_{j,k}^n$ are stored at the solution point $\overline{G}'$, (j,k,n). In Eqs. (2.6-8), $(f_m)_{j,k}^n$, $(g_m)_{j,k}^n$, $(f_{mx})_{j,k}^n$, $(g_{mx})_{j,k}^n$, $(f_{my})_{j,k}^n$ and $(g_{my})_{j,k}^n$) can be expressed by $(u_m)_{j,k}^n$, $(u_{mx})_{j,k}^n$ and $(u_{my})_{j,k}^n$. Let $\mathbf{h}_m^* = (f_m^*, g_m^*, u_m^*)$, and Eq. (2.4) can be approximated by

$$\oint_{S(V)} \mathbf{h}_m^* \cdot d\mathbf{s} = 0, \quad (2.9)$$

for m = 1, 2, 3, 4. By requiring u_m^*, f_m^* and g_m^* satisfying Eq. (2.1) inside $SE(j,k,n)$, we have

$$(u_{mt})_{j,k}^n = -(f_{mx})_{j,k}^n - (g_{my})_{j,k}^n, \quad (2.10)$$

for m = 1, 2, 3, 4. To proceed, let $f_{m,l}$ and $g_{m,l}$ be the entries of the Jacobian matrixes **F** and **G,** i.e.,

$$f_{m,l} = \frac{\partial f_m}{\partial u_l} \quad \text{and} \quad g_{m,l} = \frac{\partial g_m}{\partial u_l}, \quad (2.11)$$

for m, l = 1, 2, 3, 4. Aided by the chain rule, we have,

$$(f_{mx})_j^n = \sum_{l=1}^{4} (f_{m,l})_{j,k}^n (u_{lx})_{j,k}^n, \quad (2.12)$$

$$(f_{my})_j^n = \sum_{l=1}^{4} (f_{m,l})_{j,k}^n (u_{ly})_{j,k}^n, \quad (2.13)$$

$$(g_{mx})_{j,k}^n = \sum_{l=1}^{4} (g_{m,l})_{j,k}^n (u_{lx})_{j,k}^n, \quad (2.14)$$

$$(g_{my})_{j,k}^n = \sum_{l=1}^{4} (g_{m,l})_{j,k}^n (u_{ly})_{j,k}^n. \quad (2.15)$$

Aided by Eqs. (2.12-15), Eq. (2.10) can be recast to

$$(u_{mt})_j^n = -\sum_{l=1}^{4} (f_{m,l})_{j,k}^n (u_{lx})_{j,k}^n - \sum_{l=1}^{4} (g_{m,l})_{j,k}^n (u_{ly})_{j,k}^n, \quad (2.16)$$

Aided by the chain rule and Eqs. (2.16), $(f_{mt})_{j,k}^n$ and $(g_{mt})_{j,k}^n$ can be expressed as,

$$(f_{mt})_j^n = \sum_{l=1}^{4} (f_{m,l})_{j,k}^n (u_{lt})_{j,k}^n = -\sum_{l=1}^{4} (f_{m,l})_j^n \sum_{r=1}^{4} (f_{l,r})_{j,k}^n (u_{rx})_{j,k}^n - \sum_{l=1}^{4} (f_{m,l})_j^n \sum_{r=1}^{4} (g_{l,r})_{j,k}^n (u_{ry})_{j,k}^n, \quad (2.17)$$

$$(g_{mt})_{j,k}^n = \sum_{l=1}^{4} (g_{m,l})_{j,k}^n (u_{lt})_{j,k}^n = -\sum_{l=1}^{4} (g_{m,l})_{j,k}^n \sum_{r=1}^{4} (f_{l,r})_{j,k}^n (u_{rx})_{j,k}^n - \sum_{l=1}^{4} (g_{m,l})_{j,k}^n \sum_{r=1}^{4} (g_{l,r})_{j,k}^n (u_{ry})_{j,k}^n. \quad (2.18)$$

Aided by Eqs. (2.12-18), we could fully specify the distribution of u_m^*, f_m^* and g_m^* inside $SE(j,k,n)$ when values of $(u_m)_{j,k}^n$ $(u_{mx})_{j,k}^n$ and $(u_{my})_{j,k}^n$ are known.

2.3 Time Marching for *u*

For each m = 1, 2, 3, 4, there are three unknowns, $(u_m)_{j,k}^n$, $(u_{mx})_{j,k}^n$ and $(u_{my})_{j,k}^n$. Three CEs, i.e., $CE_1(j,k,n)$, $CE_2(j,k,n)$ and $CE_3(j,k,n)$, associated with point G', (j,k,n), are constructed to provide three algebraic equations to solve the unknowns.

To proceed, we calculate the flux leaving surfaces of CEs. Consider $CE_1(j,k,n)$, the quadrilateral cylinder $ABGFA'B'G'F'$ .The surfaces of $CE_1(j,k,n)$ can be divided into two groups. Refer to Fig. 5. Quadrilaterals $FGG'F'$, $A'B'G'F'$ and $BGG'B'$ belong to $SE(j,k,n)$, and quadrilaterals $ABGF$, $ABB'A'$ and $AFF'A'$ belong to $SE(j1,k1,n-1/2)$. Let S be the area of the quadrilaterals. Let $(x_{cen}, y_{cen}, t_{cen})$ be the coordinates of the centroid of each area. Over each area, let the outward normal vector be **n**, and the surface vector **s** = **n** S.

The flux leaving a surface is equal to the scalar product between the vector $\mathbf{h}_m^* = (f_m^*, g_m^*, u_m^*)$, evaluated at surface's centroid, and the surface vector **s**. For quadrilateral $A'B'G'F'$ in E_3, its surface vector is

$$\mathbf{s}_{A'B'G'F'} = (0, 0, S_{q1}), \quad (2.19)$$

and the coordinates of its centroid O, as shown in Fig. 5, are

$$\left(x_O, y_O, t_O\right) = \left(x_{q1}, y_{q1}, t^n\right). \tag{2.20}$$

The flux leaving the surface $A'B'G'F'$ is

$$\left(FLUX_m\right)_{A'B'G'F'} = S_{q1}\Big[\left(u_m\right)^n_{j,k} + \left(x_{q1} - x_{\overline{G}}\right)\left(u_{mx}\right)^n_{j,k} + \left(y_{q1} - y_{\overline{G}}\right)\left(u_{my}\right)^n_{j,k}\Big]. \tag{2.21}$$

For quadrilateral $FGG'F'$, its surface vector is

$$\mathbf{s}_{FGG'F'} = \frac{\Delta t}{2}\left(y_F - y_G, x_G - x_F, 0 \right), \tag{2.22}$$

and the coordinates of its centroid Q, as shown in Fig. 5, are

$$\left(x_Q, y_Q, t_Q\right) = \left(\frac{x_F + x_G}{2}, \frac{y_F + y_G}{2}, t^n - \frac{\Delta t}{4}\right). \tag{2.23}$$

The flux leaving the surface $FGG'F'$ is

$$\begin{aligned}\left(FLUX_m\right)_{FGG'F'} =\ & \frac{\Delta t}{2}\left(y_F - y_G\right)\Bigg[\left(f_m\right)^n_{j,k} + \left(\frac{x_F + x_G}{2} - x_{\overline{G}}\right)\left(f_{mx}\right)^n_{j,k} \\ & + \left(\frac{y_F + y_G}{2} - y_{\overline{G}}\right)\left(f_{my}\right)^n_{j,k} - \frac{\Delta t}{4}\left(f_{mt}\right)^n_{j,k}\Bigg] \\ & + \frac{\Delta t}{2}\left(x_G - x_F\right)\Bigg[\left(g_m\right)^n_{j,k} + \left(\frac{x_F + x_G}{2} - x_{\overline{G}}\right)\left(g_{mx}\right)^n_{j,k} \\ & + \left(\frac{y_F + y_G}{2} - y_{\overline{G}}\right)\left(g_{my}\right)^n_{j,k} - \frac{\Delta t}{4}\left(g_{mt}\right)^n_{j,k}\Bigg].\end{aligned} \tag{2.24}$$

For quadrilateral $BGG'B'$, its surface vector is

$$\mathbf{s}_{BGG'B'} = \frac{\Delta t}{2}\left(y_G - y_B, x_B - x_G, 0 \right), \tag{2.25}$$

and the coordinates of its centroid P, as shown in Fig. 5, are

$$\left(x_P, y_P, t_P\right) = \left(\frac{x_B + x_G}{2}, \frac{y_B + y_G}{2}, t^n - \frac{\Delta t}{4}\right). \tag{2.26}$$

The flux leaving the surface $BGG'B'$ is

$$\begin{aligned}\left(FLUX_m\right)_{BGG'B'} =\ & \frac{\Delta t}{2}\left(y_G - y_B\right)\Bigg[\left(f_m\right)^n_{j,k} + \left(\frac{x_B + x_G}{2} - x_{\overline{G}}\right)\left(f_{mx}\right)^n_{j,k} \\ & + \left(\frac{y_B + y_G}{2} - y_{\overline{G}}\right)\left(f_{my}\right)^n_{j,k} - \frac{\Delta t}{4}\left(f_{mt}\right)^n_{j,k}\Bigg] \\ & + \frac{\Delta t}{2}\left(x_B - x_G\right)\Bigg[\left(g_m\right)^n_{j,k} + \left(\frac{x_B + x_G}{2} - x_{\overline{G}}\right)\left(g_{mx}\right)^n_{j,k} \\ & + \left(\frac{y_B + y_G}{2} - y_{\overline{G}}\right)\left(g_{my}\right)^n_{j,k} - \frac{\Delta t}{4}\left(g_{mt}\right)^n_{j,k}\Bigg].\end{aligned} \tag{2.27}$$

The flux leaving three surfaces belonging to $SE(j,k,n)$ is the sum of Eqs. (2.21), (2.24) and (2.27). Similar calculation could be performed to obtain fluxes leaving three surfaces belonging to $SE(j1,k1,n-1/2)$, and we have

$$\begin{aligned}\left(flux_m\right)_1^{n-1/2} =\ & -S_{q1}\Big[\left(u_m\right)^{n-1/2}_{j1,k1} + \left(x_{q1} - x_{\overline{A}}\right)\left(u_{mx}\right)^{n-1/2}_{j1,k1} \\ & + \left(y_{q1} - y_{\overline{A}}\right)\left(u_{my}\right)^{n-1/2}_{j1,k1}\Big] + \frac{\Delta t}{2}\left(y_B - y_F\right)\left(f_m\right)^{n-1/2}_{j1,k1} \\ & + \frac{\Delta t}{4}\Big[\left(x_B + x_A\right)\left(y_B - y_A\right) + \left(x_F + x_A\right)\left(y_A - y_F\right) \\ & - 2x_{\overline{A}}\left(y_B - y_F\right)\Big]\left(f_{mx}\right)^{n-1/2}_{j1,k1} \\ & + \frac{\Delta t}{4}\Big[y_B^2 - y_F^2 - 2y_{\overline{A}}\left(y_B - y_F\right)\Big]\left(f_{my}\right)^{n-1/2}_{j1,k1} \\ & + \frac{(\Delta t)^2}{8}\left(y_B - y_F\right)\left(f_{mt}\right)^{n-1/2}_{j1,k1} + \frac{\Delta t}{2}\left(x_F - x_B\right)\left(g_m\right)^{n-1/2}_{j1,k1} \\ & + \frac{\Delta t}{4}\Big[x_F^2 - x_A^2 - 2x_{\overline{A}}\left(x_F - x_B\right)\Big]\left(g_{mx}\right)^{n-1/2}_{j1,k1} \\ & + \frac{\Delta t}{4}\Big[\left(x_A - x_B\right)\left(y_A + y_B\right) \\ & + \left(x_F - x_A\right)\left(y_A + y_F\right) - 2y_{\overline{A}}\left(x_F - x_B\right)\Big]\left(g_{my}\right)^{n-1/2}_{j1,k1} \\ & + \frac{(\Delta t)^2}{8}\left(x_F - x_B\right)\left(g_{mt}\right)^{n-1/2}_{j1,k1}.\end{aligned} \tag{2.28}$$

where $\left(u_m\right)^{n-1/2}_{j1,k1}$, $\left(u_{mx}\right)^{n-1/2}_{j1,k1}$ and $\left(u_{my}\right)^{n-1/2}_{j1,k1}$ are values stored at solution point $\overline{A}$. With the aid of Eqs. (2.21), (2.24), (2.27) and (2.28), the flux conservation over $CE_1(j,k,n)$ is

$$\begin{aligned}& S_{q1}\Big[\left(u_m\right)^n_{j,k} + \left(x_{q1} - x_{\overline{G}}\right)\left(u_{mx}\right)^n_{j,k} + \left(y_{q1} - y_{\overline{G}}\right)\left(u_{my}\right)^n_{j,k}\Big] \\ & + \frac{\Delta t}{2}\left(y_F - y_B\right)\left(f_m\right)^n_{j,k} + \frac{\Delta t}{4}\Big[\left(x_F + x_G\right)\left(y_F - y_G\right) \\ & - \left(x_B + x_G\right)\left(y_B - y_G\right) - 2x_{\overline{G}}\left(y_F - y_B\right)\Big]\left(f_{mx}\right)^n_{j,k} \\ & + \frac{\Delta t}{4}\Big[y_F^2 - y_B^2 - 2y_{\overline{G}}\left(y_F - y_B\right)\Big]\left(f_{my}\right)^n_{j,k} \\ & - \frac{(\Delta t)^2}{8}\left(y_F - y_B\right)\left(f_{mt}\right)^n_{j,k} + \frac{\Delta t}{2}\left(x_B - x_F\right)\left(g_m\right)^n_{j,k} \\ & + \frac{\Delta t}{4}\Big[x_B^2 - x_F^2 - 2x_{\overline{G}}\left(x_B - x_F\right)\Big]\left(g_{mx}\right)^n_{j,k} \\ & + \frac{\Delta t}{4}\Big[\left(x_B - x_G\right)\left(y_B + y_G\right) - \left(x_F - x_G\right)\left(y_F + y_G\right) \\ & - 2x_{\overline{G}}\left(y_B - y_F\right)\Big]\left(g_{my}\right)^n_{j,k} \\ & - \frac{(\Delta t)^2}{8}\left(x_B - x_F\right)\left(g_{mt}\right)^n_{j,k} + \left(flux_m\right)_1^{n-1/2} = 0,\end{aligned} \tag{2.29}$$

Similarly, the flux conservation over $CE_2(j,k,n)$ is

$$\begin{aligned}& S_{q2}\Big[\left(u_m\right)^n_{j,k} + \left(x_{q2} - x_{\overline{G}}\right)\left(u_{mx}\right)^n_{j,k} \\ & + \left(y_{q2} - y_{\overline{G}}\right)\left(u_{my}\right)^n_{j,k}\Big]\end{aligned}$$

$$+\frac{\Delta t}{2}(y_B-y_D)(f_m)^n_{j,k}+\frac{\Delta t}{4}[(x_B+x_G)(y_B-y_G)$$
$$-(x_D+x_G)(y_D-y_G)-2x_{\overline{G}}(y_B-y_D)](f_m)^n_{j,k}$$
$$+\frac{\Delta t}{4}\left[y_B^2-y_D^2-2y_{\overline{G}}(y_B-y_D)\right](f_{my})^n_{j,k}$$
$$-\frac{(\Delta t)^2}{8}(y_B-y_D)(f_{mt})^n_{j,k}+\frac{\Delta t}{2}(x_D-x_B)(g_m)^n_{j,k}$$
$$+\frac{\Delta t}{4}\left[x_D^2-x_B^2-2x_{\overline{G}}(x_D-x_B)\right](g_{mx})^n_{j,k}$$
$$+\frac{\Delta t}{4}[(x_D-x_G)(y_D+y_G)$$
$$-(x_B-x_G)(y_B+y_G)-2x_{\overline{G}}(y_D-y_B)](g_{my})^n_{j,k}$$
$$-\frac{(\Delta t)^2}{8}(x_D-x_B)(g_{mt})^n_{j,k}+(flux_m)_2^{n-1/2}=0\,. \tag{2.30}$$

where the fluxes leaving three surfaces of $SE(j2,k2,n-1/2)$ are

$$(flux_m)_2^{n-1/2}=$$
$$-S_{q2}\left[(u_m)^{n-1/2}_{j2,k2}+(x_{q2}-x_{\overline{C}})(u_{mx})^{n-1/2}_{j2,k2}\right.$$
$$\left.+(y_{q1}-y_{\overline{C}})(u_{my})^{n-1/2}_{j2,k2}\right]+\frac{\Delta t}{4}(y_D-y_B)(f_m)^{n-1/2}_{j2,k2}$$
$$+\frac{\Delta t}{4}[(x_D+x_C)(y_D-y_C)$$
$$+(x_B+x_C)(y_C-y_B)-2x_{\overline{C}}(y_D-y_B)](f_{mx})^{n-1/2}_{j2,k2}$$
$$+\frac{\Delta t}{4}\left[y_D^2-y_B^2-2y_{\overline{C}}(y_D-y_B)\right](f_{my})^{n-1/2}_{j2,k2}$$
$$+\frac{(\Delta t)^2}{8}(y_D-y_B)(f_{mt})^{n-1/2}_{j2,k2}+\frac{\Delta t}{2}(x_B-x_D)(g_m)^{n-1/2}_{j2,k2}$$
$$+\frac{\Delta t}{4}\left[x_B^2-x_D^2-2x_{\overline{C}}(x_B-x_D)\right](g_{mx})^{n-1/2}_{j2,k2}$$
$$+\frac{\Delta t}{4}[(x_B-x_C)(y_B+y_C)$$
$$+(x_C-x_D)(y_D+y_C)-2y_{\overline{C}}(x_B-x_D)](g_{my})^{n-1/2}_{j1,k1}$$
$$+\frac{(\Delta t)^2}{8}(x_B-x_D)(g_{mt})^{n-1/2}_{j1,k1}\,. \tag{2.31}$$

Similarly, the flux conservation over $CE_3(j,k,n)$ is

$$S_{q3}\left[(u_m)^n_{j,k}+(x_{q3}-x_{\overline{G}})(u_{mx})^n_{j,k}+(y_{q3}-y_{\overline{G}})(u_{my})^n_{j,k}\right]$$
$$+\frac{\Delta t}{2}(y_D-y_F)(f_m)^n_{j,k}+\frac{\Delta t}{4}[(x_D+x_G)(y_D-y_G)$$
$$-(x_F+x_G)(y_F-y_G)-2x_{\overline{G}}(y_D-y_F)](f_{mx})^n_{j,k}$$
$$+\frac{\Delta t}{4}\left[y_D^2-y_F^2-2y_{\overline{G}}(y_D-y_F)\right](f_{my})^n_{j,k}$$
$$-\frac{(\Delta t)^2}{8}(y_D-y_F)(f_{mt})^n_{j,k}+\frac{\Delta t}{2}(x_F-x_D)(g_m)^n_{j,k}$$
$$+\frac{\Delta t}{4}\left[x_F^2-x_D^2-2x_{\overline{G}}(x_F-x_D)\right](g_{mx})^n_{j,k}$$
$$+\frac{\Delta t}{4}[(x_F-x_G)(y_F+y_G)-(x_D-x_G)(y_D+y_G)$$
$$-2x_{\overline{G}}(y_F-y_D)](g_{my})^n_{j,k}$$
$$-\frac{(\Delta t)^2}{8}(x_F-x_D)(g_{mt})^n_{j,k}+(flux_m)_3^{n-1/2}=0\,, \tag{2.32}$$

where the fluxes leaving the three surfaces of $SE(j3,k3,n-1/2)$ are

$$(flux_m)_3^{n-1/2}=$$
$$-S_{q3}\left[(u_m)^{n-1/2}_{j3,k3}+(x_{q3}-x_{\overline{E}})(u_{mx})^{n-1/2}_{j3,k3}\right.$$
$$\left.+(y_{q3}-y_{\overline{E}})(u_{my})^{n-1/2}_{j3,k3}\right]+\frac{\Delta t}{2}(y_F-y_D)(f_m)^{n-1/2}_{j3,k3}$$
$$+\frac{\Delta t}{4}[(x_F+x_E)(y_F-y_E)$$
$$+(x_D+x_E)(y_E-y_D)-2x_{\overline{E}}(y_F-y_D)](f_{mx})^{n-1/2}_{j3,k3}$$
$$+\frac{\Delta t}{4}\left[y_F^2-y_D^2-2y_{\overline{E}}(y_F-y_D)\right](f_{my})^{n-1/2}_{j3,k3}$$
$$+\frac{(\Delta t)^2}{8}(y_F-y_D)(f_{mt})^{n-1/2}_{j3,k3}\quad+\frac{\Delta t}{2}(x_D-x_F)(g_m)^{n-1/2}_{j3,k3}$$
$$+\frac{\Delta t}{4}\left[x_D^2-x_F^2-2x_{\overline{E}}(x_D-x_F)\right](g_{mx})^{n-1/2}_{j3,k3}$$
$$+\frac{\Delta t}{4}[(x_D-x_E)(y_D+y_E)$$
$$+(x_E-x_F)(y_E+y_F)-2y_{\overline{E}}(x_D-x_F)](g_{my})^{n-1/2}_{j3,k3}$$
$$+\frac{(\Delta t)^2}{8}(x_D-x_F)(g_{mt})^{n-1/2}_{j3,k3}\,. \tag{2.33}$$

For each m =1, 2, 3, 4, Eqs. (2.29), (3.30) and (2.32) are the three equations, which could be used to solve for the three unknowns, $(u_m)^n_{j,k}$, $(u_{mx})^n_{j,k}$ and $(u_{my})^n_{j,k}$. Aided by Eq. (2.5), the summation of Eqs. (2.29), (2.30) and (2.32) is

$$(u_m)^n_{j,k}=$$
$$-\frac{(flux_m)_1^{n-1/2}+(flux_m)_2^{n-1/2}+(flux_m)_3^{n-1/2}}{S_{q1}+S_{q2}+S_{q3}}\,. \tag{2.34}$$

Equation (2.34) is equivalent to imposing the space-time flux conservation, i.e., Eq. (2.9) over $CE(j,k,n)$.

2.4 Time Marching for u_x and u_y

In this section, we illustrate the calculation of the spatial derivatives of the flow variables, i.e.,

$\left(u_{mx}\right)_{j,k}^{n}$ and $\left(u_{my}\right)_{j,k}^{n}$. To proceed, we subtract Eq. (2.29) from Eq. (2.30), and have

$$\sum_{l=1}^{4}\left(a1_{ml}\right)_{j,k}^{n}\left(u_{lx}\right)_{j,k}^{n}+\sum_{l=1}^{4}\left(b1_{ml}\right)_{j,k}^{n}\left(u_{ly}\right)_{j,k}^{n}=\left(c1_{m}\right)_{j,k}^{n}, \tag{2.35}$$

where $\left(a1_{ml}\right)_{j,k}^{n}$ and $\left(b1_{ml}\right)_{j,k}^{n}$ are 4×4 matrices and $\left(c1_{m}\right)_{j,k}^{n}$ is a 4×1 column vector, and they are

$$\begin{aligned}
\left(a1_{ml}\right)_{j,k}^{n} = {} & \left[S_{q2}\left(x_{q2}-x_{\overline{G}}\right)-S_{q1}\left(x_{q1}-x_{\overline{G}}\right)\right]\delta_{ml} \\
& +\frac{\Delta t}{4}\left(f_{m,l}\right)_{j,k}^{n}\left[2\left(x_B+x_G\right)\left(y_B-y_G\right)\right. \\
& \quad -\left(x_D+x_G\right)\left(y_D-y_G\right)-\left(x_F+x_G\right)\left(y_F-y_G\right) \\
& \left. -2x_{\overline{G}}\left(2y_B-y_D-y_F\right)\right] \\
& +\frac{\Delta t}{4}\left[x_D^2+x_F^2-2x_B^2-2x_{\overline{G}}\left(x_D+x_F-2x_B\right)\right]\left(g_{m,l}\right)_{j,k}^{n} \\
& -\frac{(\Delta t)^2}{8}\left(y_D+y_F-2y_B\right)\sum_{p=1}^{4}\left(f_{m,p}\right)_{j,k}^{n}\left(f_{p,l}\right)_{j,k}^{n} \\
& -\frac{(\Delta t)^2}{8}\left(2x_B-x_D-x_F\right)\sum_{p=1}^{4}\left(g_{m,p}\right)_{j,k}^{n}\left(f_{p,l}\right)_{j,k}^{n},
\end{aligned} \tag{2.36}$$

$$\begin{aligned}
\left(b1_{ml}\right)_{j,k}^{n} = {} & \left[S_{q2}\left(y_{q2}-y_{\overline{G}}\right)-S_{q1}\left(y_{q1}-y_{\overline{G}}\right)\right]\delta_{ml} \\
& +\frac{\Delta t}{4}\left[2y_B^2-y_D^2-y_F^2\right. \\
& \quad \left.-2y_{\overline{G}}\left(2y_B-y_F-y_D\right)\right]\left(f_{m,l}\right)_{j,k}^{n} \\
& +\frac{\Delta t}{4}\left(g_{m,l}\right)_{j,k}^{n}\left[\left(x_D-x_G\right)\left(y_D+y_G\right)\right. \\
& +\left(x_F-x_G\right)\left(y_F+y_G\right)-2\left(x_B-x_G\right)\left(y_B+y_G\right) \\
& \left.-2y_{\overline{G}}\left(x_D+x_F-2x_B\right)\right] \\
& -\frac{(\Delta t)^2}{8}\left(y_D+y_F-2y_B\right)\sum_{p=1}^{4}\left(f_{m,p}\right)_{j,k}^{n}\left(g_{p,l}\right)_{j,k}^{n} \\
& -\frac{(\Delta t)^2}{8}\left(2x_B-x_D-x_F\right)\sum_{p=1}^{4}\left(g_{m,p}\right)_{j,k}^{n}\left(g_{p,l}\right)_{j,k}^{n},
\end{aligned} \tag{2.37}$$

and

$$\begin{aligned}
\left(c1_{m}\right)_{j,k}^{n} = {} & \left(flux_m\right)_1^{n-1/2}-\left(flux_m\right)_2^{n-1/2} \\
& +\left(S_{q1}-S_{q2}\right)\left(u_m\right)_{j,k}^{n}-\frac{\Delta t}{2}\left(2y_B-y_D-y_F\right)\left(f_m\right)_{j,k}^{n} \\
& -\frac{\Delta t}{2}\left(x_D+x_F-2x_B\right)\left(g_m\right)_{j,k}^{n}.
\end{aligned} \tag{2.38}$$

Similarly, we subtract Eq. (2.29) from Eq. (2.32), and we have

$$\sum_{l=1}^{4}\left(a2_{ml}\right)_{j,k}^{n}\left(u_{lx}\right)_{j,k}^{n}+\sum_{l=1}^{4}\left(b2_{ml}\right)_{j,k}^{n}\left(u_{ly}\right)_{j,k}^{n}=\left(c2_{m}\right)_{j,k}^{n}, \tag{2.39}$$

where

$$\begin{aligned}
\left(a2_{ml}\right)_{j,k}^{n} = {} & \left[S_{q3}\left(x_{q3}-x_{\overline{G}}\right)-S_{q1}\left(x_{q1}-x_{\overline{G}}\right)\right]\delta_{ml} \\
& +\frac{\Delta t}{4}\left(f_{m,l}\right)_{j,k}^{n}\left[\left(x_B+x_G\right)\left(y_B-y_G\right)\right. \\
& +\left(x_D+x_G\right)\left(y_D-y_G\right)-2\left(x_F+x_G\right)\left(y_F-y_G\right) \\
& \quad \left.-2x_{\overline{G}}\left(2y_F-y_B-y_D\right)\right] \\
& +\frac{\Delta t}{4}\left[2x_F^2-x_B^2-x_D^2\right. \\
& \quad \left.-2x_{\overline{G}}\left(2x_F-x_B-x_D\right)\right]\left(g_{m,l}\right)_{j,k}^{n} \\
& -\frac{(\Delta t)^2}{8}\left(2y_F-y_B+y_D\right)\sum_{p=1}^{4}\left(f_{m,p}\right)_{j,k}^{n}\left(f_{p,l}\right)_{j,k}^{n} \\
& -\frac{(\Delta t)^2}{8}\left(x_B+x_D-2x_F\right)\sum_{p=1}^{4}\left(g_{m,p}\right)_{j,k}^{n}\left(f_{p,l}\right)_{j,k}^{n},
\end{aligned} \tag{2.40}$$

$$\begin{aligned}
\left(b2_{ml}\right)_{j,k}^{n} = {} & \left[S_{q3}\left(y_{q3}-y_{\overline{G}}\right)-S_{q1}\left(y_{q1}-y_{\overline{G}}\right)\right]\delta_{ml} \\
& +\frac{\Delta t}{4}\left(f_{m,l}\right)_{j,k}^{n}\left[y_B^2+y_D^2-2y_F^2\right. \\
& \quad \left.-2y_{\overline{G}}\left(y_D+y_B-2y_F\right)\right] \\
& +\frac{\Delta t}{4}\left(g_{m,l}\right)_{j,k}^{n}\left[2\left(x_F-x_G\right)\left(y_F+y_G\right)\right. \\
& -\left(x_B-x_G\right)\left(y_B+y_G\right)-\left(x_D-x_G\right)\left(y_D+y_G\right)] \\
& \left.-2y_{\overline{G}}\left(2x_F-x_B-x_D\right)\right] \\
& -\frac{(\Delta t)^2}{8}\left(2y_F-y_B-y_D\right)\sum_{p=1}^{4}\left(f_{m,p}\right)_{j,k}^{n}\left(g_{p,l}\right)_{j,k}^{n} \\
& -\frac{(\Delta t)^2}{8}\left(x_B+x_D-2x_F\right)\sum_{p=1}^{4}\left(g_{m,p}\right)_{j,k}^{n}\left(g_{p,l}\right)_{j,k}^{n},
\end{aligned} \tag{2.41}$$

$$\begin{aligned}
\left(c2_{m}\right)_{j,k}^{n} = {} & \left(flux_m\right)_1^{n-1/2}-\left(flux_m\right)_3^{n-1/2} \\
& +\left(S_{q1}-S_{q3}\right)\left(u_m\right)_{j,k}^{n}-\frac{\Delta t}{2}\left(y_B+y_D-2y_F\right)\left(f_m\right)_{j,k}^{n} \\
& -\frac{\Delta t}{2}\left(2x_F-x_B-x_D\right)\left(g_m\right)_{j,k}^{n}.
\end{aligned} \tag{2.42}$$

For each m = 1, 2, 3, 4, Eqs. (2.35) and (2.39) provide two equations for two unknowns, i.e., $\left(u_{mx}\right)_{j,k}^{n}$ and $\left(u_{my}\right)_{j,k}^{n}$.

The combination of Eq. (2.34) for $(u_m)_{j,k}^n$ and Eqs. (2.35,39) for $(u_{mx})_{j,k}^n$ and $(u_{my})_{j,k}^n$ form the *a* scheme of the two-dimensional CESE method. In the following, $(u_{mx})_{j,k}^n$ and $(u_{my})_{j,k}^n$ calculated by the *a* scheme, i.e., Eqs. (2.35) and (2.39), are referred to as $(u_{mx}^a)_{j,k}^n$ and $(u_{my}^a)_{j,k}^n$.

2.5 The *a*-ε-α Scheme for Shock Capturing

For solutions with discontinuities, further modification for the calculation of $(u_{mx})_{j,k}^n$ and $(u_{my})_{j,k}^n$ is needed. The above *a* scheme will be extended to the *a*-ε and the *a*-ε-α-β schemes.

We note that point $\overline{G}'$ is not the centroid of $\Delta\overline{A}'\overline{C}'\overline{E}'$ unless a uniform mesh is used. As shown in Fig. 6, a triangle $\Delta A^*C^*E^*$, whose centroid is point $\overline{G}'$, is obtained by parallel moving $\Delta\overline{A}'\overline{C}'\overline{E}'$ in the spatial domain. The vertices' coordinates of $\Delta A^*C^*E^*$ are

$$x_{A^*} = (3x_{\overline{G}} + 2x_{\overline{A}} - x_{\overline{C}} - x_{\overline{E}})/3, \quad y_{A^*} = (3y_{\overline{G}} + 2y_{\overline{A}} - y_{\overline{C}} - y_{\overline{E}})/3, \tag{2.43}$$

$$x_{C^*} = (3x_{\overline{G}} + 2x_{\overline{C}} - x_{\overline{A}} - x_{\overline{E}})/3, \quad y_{C^*} = (3y_{\overline{G}} + 2y_{\overline{C}} - y_{\overline{A}} - y_{\overline{E}})/3, \tag{2.44}$$

$$x_{E^*} = (3x_{\overline{G}} + 2x_{\overline{E}} - x_{\overline{A}} - x_{\overline{C}})/3, \quad y_{E^*} = (3y_{\overline{G}} + 2y_{\overline{E}} - y_{\overline{A}} - y_{\overline{C}})/3. \tag{2.45}$$

Flow variables at $\overline{G}'$, i.e., $(u_m)_{j,k}^n$, are calculated from Eq. (2.34). Flow variable at point A^* is obtained by a first-order Taylor series expansion

$$(u_m')_{j1,k1}^n = (u_m)_{j1,k1}^{n-1/2} + \frac{\Delta t}{2}(u_{mt})_{j1,k1}^{n-1/2} + (x_{A^*} - x_{\overline{A}})(u_{mx})_{j1,k1}^{n-1/2} + (y_{A^*} - y_{\overline{A}})(u_{my})_{j1,k1}^{n-1/2}. \tag{2.46}$$

Similarly, $(u_m')_{j2,k2}^n$ and $(u_m')_{j3,k3}^n$, at C^* and E^* can be obtained. Based on $(u_m')_{j1,k1}^n$, $(u_m')_{j2,k2}^n$ and $(u_m')_{j3,k3}^n$ on points A^*, C^* and E^*, we apply central differencing to calculate $(u_{mx})_{j,k}^n$ and $(u_{my})_{j,k}^n$ at point $\overline{G}'$, i.e.,

$$(u_{mx}^c)_{j,k}^n = \frac{1}{2S_{A^*C^*E^*}}\Big[(y_{C^*} - y_{E^*})(u_m')_{j1,k1}^n + (y_{E^*} - y_{A^*})(u_m')_{j2,k2}^n + (y_{A^*} - y_{C^*})(u_m')_{j3,k3}^n\Big], \tag{2.47}$$

$$(u_{my}^c)_{j,k}^n = \frac{1}{2S_{A^*C^*E^*}}\Big[(x_{E^*} - x_{C^*})(u_m')_{j1,k1}^n + (x_{A^*} - x_{E^*})(u_m')_{j2,k2}^n + (x_{C^*} - x_{A^*})(u_m')_{j3,k3}^n\Big], \tag{2.48}$$

where $S_{\Delta A^*C^*E^*}$ is the area of $\Delta A^*C^*E^*$:

$$S_{\Delta A^*C^*E^*} = \frac{1}{2}(x_{A^*}y_{C^*} + x_{C^*}y_{E^*} + x_{E^*}y_{A^*} - x_{A^*}y_{E^*} - x_{C^*}y_{A^*} - x_{E^*}y_{C^*}). \tag{2.49}$$

Similar central differencing can be applied to calculate $(u_{mx}^{(1)})_{j,k}^n$ and $(u_{my}^{(1)})_{j,k}^n$ for $\Delta C^*E^*\overline{G}'$, $(u_{mx}^{(2)})_{j,k}^n$ and $(u_{my}^{(2)})_{j,k}^n$ for $\Delta A^*\overline{G}'E^*$, and $(u_{mx}^{(3)})_{j,k}^n$ and $(u_{my}^{(3)})_{j,k}^n$ for $\Delta A^*C^*\overline{G}'$. Moreover, because point $\overline{G}'$ is the centroid of $\Delta A^*C^*E^*$,

$$(u_{mx}^c)_{j,k}^n = \frac{1}{3}\sum_{r=1}^{3}(u_{mx}^{(r)})_{j,k}^n$$

$$(u_{my}^c)_{j,k}^n = \frac{1}{3}\sum_{r=1}^{3}(u_{my}^{(r)})_{j,k}^n. \tag{2.50}$$

Aided by Eqs. (2.47-48), $(u_{mx})_{j,k}^n$ and $(u_{my})_{j,k}^n$ for the *a*-*ε* scheme are

$$(u_{mx})_{j,k}^n = (u_{mx}^a)_{j,k}^n + 2\varepsilon\Big[(u_{mx}^c)_{j,k}^n - (u_{mx}^a)_{j,k}^n\Big], \tag{2.51}$$

$$(u_{my})_{j,k}^n = (u_{my}^a)_{j,k}^n + 2\varepsilon\Big[(u_{my}^c)_{j,k}^n - (u_{my}^a)_{j,k}^n\Big], \tag{2.52}$$

for *m* = 1, 2, 3, 4. For numerical stability we must have $0 \le \varepsilon \le 1$. For the *a*-*ε*-*α*-*β* scheme,

$$(u_{mx})_{j,k}^n = (u_{mx}^a)_{j,k}^n + 2\varepsilon\Big[(u_{mx}^c)_{j,k}^n - (u_{mx}^a)_{j,k}^n\Big] + \beta\Big[(u_{mx}^w)_{j,k}^n - (u_{mx}^c)_{j,k}^n\Big], \tag{2.53}$$

$$(u_{my})_{j,k}^n = (u_{my}^a)_{j,k}^n + 2\varepsilon\Big[(u_{my}^c)_{j,k}^n - (u_{my}^a)_{j,k}^n\Big] + \beta\Big[(u_{my}^w)_{j,k}^n - (u_{my}^c)_{j,k}^n\Big], \tag{2.54}$$

where

$$(u_{mx}^w)_{j,k}^n = \frac{1}{\omega}\Big[(\theta_{m2}\theta_{m3})^\alpha(u_{mx}^{(1)})_{j,k}^n + (\theta_{m1}\theta_{m3})^\alpha(u_{mx}^{(2)})_{j,k}^n + (\theta_{m1}\theta_{m2})^\alpha(u_{mx}^{(3)})_{j,k}^n\Big]. \tag{2.55}$$

$$(u_{my}^w)_{j,k}^n = \frac{1}{\omega}\Big\{(\theta_{m2}\theta_{m3})^\alpha(u_{my}^{(1)})_{j,k}^n + (\theta_{m1}\theta_{m3})^\alpha(u_{my}^{(2)})_{j,k}^n + (\theta_{m1}\theta_{m2})^\alpha(u_{my}^{(3)})_{j,k}^n\Big\}. \tag{2.56}$$

and

$$\theta_{mr} = \left[\sqrt{\left(u_{mx}^{(r)}\right)^2 + \left(u_{my}^{(r)}\right)^2} \right]_{j,k}^{n}, \tag{2.57}$$

$$\omega = \left(\theta_{m1}\theta_{m2}\right)^{\alpha} + \left(\theta_{m2}\theta_{m3}\right)^{\alpha} + \left(\theta_{m1}\theta_{m3}\right)^{\alpha}. \tag{2.58}$$

For numerical stability, $\beta \geq 0$.

The above CESE schemes are stable for CFL number < 1., while $0 \leq \varepsilon \leq 1$, α≥0 and β≥0. Let ε = 0.5 and β = 1, Eqs. (2.53-54) reduce to

$$\left(u_{mx}\right)_{j,k}^{n} = \left(u_{mx}^{w}\right)_{j,k}^{n} \text{ and } \left(u_{my}\right)_{j,k}^{n} = \left(u_{my}^{w}\right)_{j,k}^{n}. \tag{2.59}$$

Equations (2.34) and (2.59) form the a-α scheme, which is the simplest and most commonly used CESE method.

3. The CFL Condition

The CFL number in two spatial dimensions is defined according to [10]. The spatial projections of solution points are presented in Fig. 7, in which solid squares are at time level $n = 0, 1, 2, \ldots$, and hollow squares are at $n = 1/2,\ 3/2, 5/2, \ldots$. According to the CESE method, the flow variables at solution point $\overline{G}'$ (*j, k, n*) are determined by those at seven solution points $\overline{A}$, $\overline{B}$, $\overline{C}$, $\overline{D}$, $\overline{E}$, $\overline{F}$ and $\overline{G}$ at the time level *n*-1. The hexagon $\overline{A}\overline{B}\overline{C}\overline{D}\overline{E}\overline{F}$ is the numerical domain of dependence for the solution at $\overline{G}'$ at time level *n*-1.

Figure 8 shows a Mach cone, with point $\overline{G}$ being its vertex, intersecting the plane *t = (n-1)Δt*. The result is a circle with a radius of *c*Δ*t* on the plane with *P* as the center of the circle. The boundary and interior of the circle form the domain of dependence for the flow solution at $\overline{G}'$. Thus, the CFL condition for the solution at $\overline{G}$ is defined such that if and only if the domain of dependence, i.e., the circle, lies in the interior of the hexagon $\overline{A}\overline{B}\overline{C}\overline{D}\overline{E}\overline{F}$. Let *u, v* and *c* be velocity components and sonic speed at solution point $\overline{G}$ at time level *n*-1. As shown in Fig. 8, for the velocity vector $\overrightarrow{\overline{G}O}$, we have

$$\left|\overline{G}O\right| = \Delta t\sqrt{u^2 + v^2} \quad \text{and} \quad \theta_0 = \arctan(v/u). \tag{3.1}$$

Let line segment $\overline{G}H$ be the distance from point $\overline{G}$ to boundary $\overline{A}\overline{B}$, we have

$$\left|\overline{G}H\right| = 2S_{\Delta\overline{A}\overline{B}\overline{G}} \Big/ \sqrt{\left(x_{\overline{B}} - x_{\overline{A}}\right)^2 + \left(y_{\overline{B}} - y_{\overline{A}}\right)^2},$$

$$\theta_1 = \arctan\frac{x_{\overline{A}} - x_{\overline{B}}}{y_{\overline{B}} - y_{\overline{A}}}. \tag{3.2}$$

As shown in Fig. 8, we choose a point *P* on the circle such that the line segment *OP* is parallel to line segment $\overline{G}H$. Let *R* and S be the projection of *O* and *P* on $\overline{G}H$. Obviously P is the closest point to the boundary $\overline{A}\overline{B}$ on the circle. To keep the circle inside the hexagon, with $\overline{A}\overline{B}$ as one of the boundary segments, we require that

$$v^{(1)} = \left|\overline{G}S\right| / \left|\overline{G}H\right| < 1, \tag{3.3}$$

where

$$\left|\overline{G}S\right| = \Delta t\left[c + \sqrt{u^2 + v^2}\cos\left(\theta_1 - \theta_0\right)\right]. \tag{3.4}$$

For the other five boundary line segments, we have similar conditions, i.e., $v^{(2)}$ for $\overline{B}\overline{C}$, $v^{(3)}$ for $\overline{C}\overline{D}$, $v^{(4)}$ for $\overline{D}\overline{E}$, $v^{(5)}$ for $\overline{E}\overline{F}$, and $v^{(6)}$ for $\overline{F}\overline{A}$. The CFL conditions is that,

$$v_e = \max\left\{v^{(1)}, v^{(2)}, v^{(3)}, v^{(4)}, v^{(5)}, v^{(6)}\right\}. \tag{3.5}$$

$$v_e < 1. \tag{3.6}$$

Essentially, Eqs. (3.5-6) specify that the domain of dependence of the flow solution at $\overline{G}$ must lies within its numerical domain of dependence, i.e., hexagon $\overline{A}\overline{B}\overline{C}\overline{D}\overline{E}\overline{F}$. In computation, Δt is chosen to satisfy Eq. (3.5-6).

4. The CFL-Insensitive CESE Method

4.1 Scheme I

To construct a CFL-insentive scheme, we re-plot $\Delta A^{*}C^{*}E^{*}$ with its centroid $\overline{G}'$ in Fig. 9 (refer to Fig. 6), where M_1, M_2 and M_3 are midpoints of line segments $\overline{G}'A^{*}$, $\overline{G}'C^{*}$ and $\overline{G}'E^{*}$, respectively. Values at points P_1, P_2 and P_3 are obtained as

$$\left(\overline{u}_m\right)'_{p_1} = \left(u'_m\right)_{j1,k1}^{n-1/2} + \frac{\Delta t}{2}\left(u_{mt}\right)_{j1,k1}^{n-1/2} + \left(1 - v_e\right)\left[\frac{x_{\overline{G}} - x_{A^{*}}}{2}\left(u_{mx}\right)_{j1,k1}^{n-1/2} + \frac{y_{\overline{G}} - y_{A^{*}}}{2}\left(u_{my}\right)_{j1,k1}^{n-1/2}\right], \tag{4.1}$$

$$\left(\overline{u}_m\right)'_{p2} = \left(u'_m\right)_{j2,k2}^{n-1/2} + \frac{\Delta t}{2}\left(u_{mt}\right)_{j2,k2}^{n-1/2} + \left(1 - v_e\right)\left[\frac{x_{\overline{G}} - x_{C^{*}}}{2}\left(u_{mx}\right)_{j2,k2}^{n-1/2} + \frac{y_{\overline{G}} - y_{C^{*}}}{2}\left(u_{my}\right)_{j2,k2}^{n-1/2}\right], \tag{4.2}$$

$$\left(\overline{u}_m\right)'_{p3} = \left(u'_m\right)_{j3,k3}^{n-1/2} + \frac{\Delta t}{2}\left(u_{mt}\right)_{j3,k3}^{n-1/2} + \left(1 - v_e\right)\left[\frac{x_{\overline{G}} - x_{E^{*}}}{2}\left(u_{mx}\right)_{j3,k3}^{n-1/2} + \frac{y_{\overline{G}} - y_{E^{*}}}{2}\left(u_{my}\right)_{j3,k3}^{n-1/2}\right], \tag{4.3}$$

The spatial coordinates of points P_1, P_2 and P_3 are defined as

$$x_{p1}=\frac{1-v_e}{2}x_{\overline{G}}+\frac{1+v_e}{2}x_{A^*},\quad y_{p1}=\frac{1-v_e}{2}y_{\overline{G}}+\frac{1+v_e}{2}y_{A^*} \tag{4.4}$$

$$x_{p2}=\frac{1-v_e}{2}x_{\overline{G}}+\frac{1+v_e}{2}x_{C^*},\quad y_{p2}=\frac{1-v_e}{2}y_{\overline{G}}+\frac{1+v_e}{2}y_{C^*} \tag{4.5}$$

$$x_{p3}=\frac{1-v_e}{2}x_{\overline{G}}+\frac{1+v_e}{2}x_{E^*},\quad y_{p3}=\frac{1-v_e}{2}y_{\overline{G}}+\frac{1+v_e}{2}y_{E^*}. \tag{4.6}$$

As v_e decreases from 1 to 0, we move P_1 from point A^* to M_1, P_2 from C^* to M_2, and P_3 from E^* to M_3. Point $\overline{G}'$ is still the centroid of $\Delta P_1P_2P_3$. By central differencing, we have

$$\left(\overline{u}^c_{mx}\right)^n_{j,k}=\frac{1}{2S_{\Delta P_1P_2P_3}}\Big[(y_{p1}-y_{p2})(\overline{u}_m)'_{p_3}+(y_{p2}-y_{p3})(\overline{u}_m)'_{p_1}+(y_{p3}-y_{p1})(\overline{u}_m)'_{p_2}\Big], \tag{4.7}$$

$$\left(\overline{u}^c_{my}\right)^n_{j,k}=\frac{-1}{2S_{\Delta P_1P_2P_3}}\Big[(x_{p1}-x_{p2})(\overline{u}_m)'_{p_3}+(x_{p2}-x_{p3})(\overline{u}_m)'_{p_1}+(x_{p3}-x_{p1})(\overline{u}_m)'_{p_2}\Big], \tag{4.8}$$

for m =1, 2, 3, 4. Similar expression can be obtained for $\left(\overline{u}^{(1)}_{mx}\right)^n_{j,k}$ and $\left(\overline{u}^{(1)}_{my}\right)^n_{j,k}$ for $\Delta\overline{G}'P_2P_3$, $\left(\overline{u}^{(2)}_{mx}\right)^n_{j,k}$ and $\left(\overline{u}^{(2)}_{my}\right)^n_{j,k}$ for $\Delta\overline{G}'P_3P_1$, and $\left(\overline{u}^{(3)}_{mx}\right)^n_{j,k}$ and $\left(\overline{u}^{(3)}_{my}\right)^n_{j,k}$ for $\Delta\overline{G}'P_1P_2$. Moreover, Eqs. (4.7-8) can be expressed as a simple average as

$$\left(\overline{u}^c_{mx}\right)^n_{j,k}=\frac{1}{3}\sum_{r=1}^{3}\left(\overline{u}^{(r)}_{mx}\right)^n_{j,k}, \tag{4.9}$$

$$\left(\overline{u}^c_{my}\right)^n_{j,k}=\frac{1}{3}\sum_{r=1}^{3}\left(\overline{u}^{(r)}_{my}\right)^n_{j,k}, \tag{4.10}$$

The re-weighted values of $\left(\overline{u}^w_{mx}\right)^n_{j,k}$ and $\left(\overline{u}^w_{mx}\right)^n_{j,k}$ are obtained by replacing $\left(u^{(1)}_{mx}\right)^n_{j,k}$, $\left(u^{(1)}_{my}\right)^n_{j,k}$, $\left(u^{(2)}_{mx}\right)^n_{j,k}$, $\left(u^{(2)}_{my}\right)^n_{j,k}$, $\left(u^{(3)}_{mx}\right)^n_{j,k}$ and $\left(u^{(3)}_{my}\right)^n_{j,k}$ in Eqs. (2.55-59) by $\left(\overline{u}^{(1)}_{mx}\right)^n_{j,k}$, $\left(\overline{u}^{(1)}_{my}\right)^n_{j,k}$, $\left(\overline{u}^{(2)}_{mx}\right)^n_{j,k}$, $\left(\overline{u}^{(2)}_{my}\right)^n_{j,k}$, $\left(\overline{u}^{(3)}_{mx}\right)^n_{j,k}$ and $\left(\overline{u}^{(3)}_{my}\right)^n_{j,k}$, respectively. The new scheme, referred as Scheme I, is

$$\left(u_{mx}\right)^n_{j,k}=\left(\overline{u}^w_{mx}\right)^n_{j,k}$$

$$\left(u_{my}\right)^n_{j,k}=\left(\overline{u}^w_{my}\right)^n_{j,k}, \tag{4.11}$$

while the calculation of $\left(u_m\right)^n_{j,k}$ remains the same in the original CESE method, i.e., by Eq. (2.34). As will be shown in Section 5, Scheme I performs better than the original CESE method with less damping when the CFL number is small. However, spurious oscillations appear near shock waves. To suppress these overshoots, we proposed Scheme II in the following section.

4.2 Scheme II

To proceed, we define,

$$\phi_{m1}=\theta_{m2}\theta_{m3},\ \phi_{m2}=\theta_{m1}\theta_{m3}\ \text{and}\ \phi_{m3}=\theta_{m2}\theta_{m1}, \tag{4.12}$$

where

$$\theta_{mr}=\left[\sqrt{\left(\overline{u}^{(r)}_{mx}\right)^2+\left(\overline{u}^{(r)}_{my}\right)^2}\right]^n_{j,k}. \tag{4.13}$$

Moreover, we let

$$\left(s_{mr}\right)^n_{j,k}=\frac{\phi_{mr}}{\min(\phi_{m1},\phi_{m2},\phi_{m3})}-1, \tag{4.14}$$

for r = 1, 2, 3. According to Eqs. (2.56-57), we define

$$\left(\overline{u}^w_{mx}\right)^n_{j,k}=\frac{1}{c}\Big\{\left[1+(s_{m1})^n_{j,k}\right]^\alpha\left(\overline{u}^{(1)}_{mx}\right)^n_{j,k}+\left[1+(s_{m2})^n_{j,k}\right]^\alpha\left(\overline{u}^{(2)}_{mx}\right)^n_{j,k}+\left[1+(s_{m3})^n_{j,k}\right]^\alpha\left(\overline{u}^{(3)}_{mx}\right)^n_{j,k}\Big\}, \tag{4.15}$$

$$\left(\overline{u}^w_{my}\right)^n_{j,k}=\frac{1}{c}\Big\{\left[1+(s_{m1})^n_{j,k}\right]^\alpha\left(\overline{u}^{(1)}_{my}\right)^n_{j,k}+\left[1+(s_{m2})^n_{j,k}\right]^\alpha\left(\overline{u}^{(2)}_{my}\right)^n_{j,k}+\left[1+(s_{m3})^n_{j,k}\right]^\alpha\left(\overline{u}^{(3)}_{my}\right)^n_{j,k}\Big\}, \tag{4.16}$$

where

$$c=\left[1+(s_{m1})^n_{j,k}\right]^\alpha+\left[1+(s_{m2})^n_{j,k}\right]^\alpha+\left[1+(s_{m3})^n_{j,k}\right]^\alpha. \tag{4.17}$$

For $\left(s_{mr}\right)^n_{j,k}$ « 1, Eqs. (4.15-16) imply that

$$\left(\overline{u}^w_{mx}\right)^n_0\approx\frac{1}{d}\Big\{\left[1+\alpha(s_{m1})^n_{j,k}\right]\left(\overline{u}^{(1)}_{mx}\right)^n_{j,k}+\left[1+\alpha(s_{m2})^n_{j,k}\right]\left(\overline{u}^{(2)}_{mx}\right)^n_{j,k}+\left[1+\alpha(s_{m3})^n_{j,k}\right]\left(\overline{u}^{(3)}_{mx}\right)^n_{j,k}\Big\}, \tag{4.18}$$

$$\left(\overline{u}^w_{my}\right)^n_0\approx\frac{1}{d}\Big\{\left[1+\alpha(s_{m1})^n_{j,k}\right]\left(\overline{u}^{(1)}_{my}\right)^n_{j,k}+\left[1+\alpha(s_{m2})^n_{j,k}\right]\left(\overline{u}^{(2)}_{my}\right)^n_{j,k}+\left[1+\alpha(s_{m3})^n_{j,k}\right]\left(\overline{u}^{(3)}_{my}\right)^n_{j,k}\Big\}, \tag{4.19}$$

where

$$d=3+\alpha\left[(s_{m1})^n_{j,k}+(s_{m2})^n_{j,k}+(s_{m3})^n_{j,k}\right], \tag{4.20}$$

To proceed, we replace α by a function $f(v_e)$:

$$\left(\overline{u}_{mx}^{w}\right)_{j,k}^{n} \approx \frac{1}{e}\left\{\left[1+f(v_e)(s_{m1})_{j,k}^{n}\right]\left(\overline{u}_{mx}^{(1)}\right)_{j,k}^{n} + \left[1+f(v_e)(s_{m2})_{j,k}^{n}\right]\left(\overline{u}_{mx}^{(2)}\right)_{j,k}^{n} + \left[1+f(v_e)(s_{m3})_{j,k}^{n}\right]\left(\overline{u}_{mx}^{(3)}\right)_{j,k}^{n}\right\}, \quad (4.21)$$

$$\left(\overline{u}_{my}^{w}\right)_{j,k}^{n} \approx \frac{1}{e}\left\{\left[1+f(v_e)(s_{m1})_{j,k}^{n}\right]\left(\overline{u}_{my}^{(1)}\right)_{j,k}^{n} + \left[1+f(v_e)(s_{m2})_{j,k}^{n}\right]\left(\overline{u}_{my}^{(2)}\right)_{j,k}^{n} + \left[1+f(v_e)(s_{m3})_{j,k}^{n}\right]\left(\overline{u}_{my}^{(3)}\right)_{j,k}^{n}\right\} \quad (4.22)$$

where

$$e = 3 + f(v_e)\left[(s_{m1})_{j,k}^{n} + (s_{m2})_{j,k}^{n} + (s_{m3})_{j,k}^{n}\right], \quad (4.23)$$

and

$$f(v_e) = 1/v_e \ . \quad (4.24)$$

Scheme II is similar to Scheme I except $\left(\overline{u}_{mx}^{w}\right)_{j,k}^{n}$ and $\left(\overline{u}_{my}^{w}\right)_{j,k}^{n}$ are obtained by Eqs. (4.21-22).

5. Numerical Results

We solve the steady oblique shock reflection problem [11] to test the above CFL-insentive CESE schemes. The computation domain is a rectangle, i.e., 1<x<4 and 0<y<1. The lower boundary is a solid wall. The computational domain and shock locations are shown in Fig. 10. The flow conditions at the left (AB) and upper (AD) boundaries are specified to stage the incident shock. The non-reflect boundary condition is employed at the right boundary (CD). The solid wall boundary condition is used on the lower boundary (BC). A 100×40 mesh is used. We use a uniform mesh and a non-uniform mesh for the calculation.

5.1 Solution with Uniform Mesh

Let Δt = 0.01, 0.001, and 0.0001, and the maximum CFL numbers in the computational domain are approximately 0.7, 0.07 and 0.007, respectively. Figure 11a shows the pressure coefficient distribution along the line y = 0.5 by the original CESE scheme. Figures 11b-11d show the pressure contours obtained by using different schemes. The contours were plotted by using the same level increments. With decreasing CFL numbers, the numerical resolution of shock waves decays significantly.

Figure 12 shows the numerical solution by using Scheme I. Contrast to the result in Fig. 11, Scheme I improves the capabilities of shocks capturing and the numerical resolution of the shock wave is nearly independent of Δt. However, overshoots appear near shock waves when CFL number = 0.007. To suppress numerical overshoots, numerical results by using Scheme II are shown in Figure 13. Shock related spurious wiggles have been effectively suppressed. Between the two CFL insensitive schemes, Scheme II performs better.

5.2 Solution of Non-Uniform Mesh

For non-uniform mesh, the grid points are clustered in the *y* direction towards the upper boundary. In *y* direction, $\Delta y_{\max}/\Delta y_{\min} \approx 30$. This arrangement was chosen to maintain the correct incident shock condition. By letting Δt = 0.001, the CFL number ranges from 0.03 to 0.6 in the computational domain. For comparison between different schemes, pressure coefficient distribution along the lines of *y* = 0.6025, *y* = 0.3350, and *y* =0.1960 are plotted in Fig. 14. Figure 15 shows the pressure contours calculated by using different schemes. Very diffusive solution is obtained by using the original scheme. The original scheme fails to capture shock at line *y* = 0.1960. On the other hand, new CFL-insensitive schemes improve solution. However, Scheme I shows overshoots near shock. Based on the above two-dimensional results, it is clear that the new schemes are insensitive to the values of the local CFL numbers, and, as a result, perform well in shock capturing for a wide range of CFL numbers. In particular, Scheme II is effective in suppressing spurious oscillations near the shock waves.

6. Concluding Remarks

Because the original CESE solution may become overly dissipative when the local CFL number is very small, Chang [9] developed new CFL number insensitive schemes for the Euler equations in one spatial dimension. In the present paper, these CFL insensitive methods have been extended for the flow equations in two spatial dimensions. The CFL condition has been illustrated by the domain dependence of the hyperbolic solutions in the space-time domain. The new CFL insensitive methods were developed by moving the mesh nodes inwards in calculating the spatial derivatives of the flow solutions. Two schemes were developed, Scheme I and II, with different treatments in the re-weighting procedure for shock capturing. Based on the numerical experiments by solving the oblique shock reflection problem, we showed that the numerical solutions of the new CESE schemes are indeed independent of local CFL numbers, and shocks were sharply resolved for a wide range of CFL numbers. The present new CESE schemes are a steppingstone for high-fidelity solution of multi-dimensional problems based on the use of severely clustered mesh near the wall.

References

1. Chang, S.C. and To, W. M., "A New Numerical Framework for Solving Conservation Laws – The Method of Space-Time Conservation Element and Solution Element", NASA TM 104498, 1991.
2. Chang, S. C., "The Method of Space-time Conservation Element and Solution Element–A New Approach for Solving the Navier-Stokes and the Euler Equations", Journal of Computational Physics, vol. 119, 1995, pp 295-324.
3. Chang, S. C., Wang, X.Y. and Chow, C.Y., "The Space-Time Conservation Element and Solution Element Method: A New High-Resolution and Genuinely Multidimensional Paradigm for Solving Conservation Laws", Journal of Computational Physics, 156, 1999, pp. 89-136.
4. Wang, X. Y. and Chang, S. C., "A 2D Non-splitting Unstructured Triangular Mesh Euler Solver Based on the Space-time Conservation Element and Solution Element Method", Computational Fluid Dynamics Journal, vol. 8, No. 2, 1999, pp.309-325.
5. Chang, S. C., Wang, X.Y. and To, W.M., "Application of the Space-time Conservation Element and Solution Element Method to One-Dimensional Convection-Diffusion Problems", Journal of Computational Physics, vol. 165 (2000) pp. 189-215.
6. Zhang, Z.C., Yu, S. T. and Chang, S. C., "A Space-Time Conservation Element and Solution Element Method for Solving the Two- and Three-Dimensional Unsteady Euler Equations Using Quadrilateral and Hexahedral Meshes", Journal of Computational Physics., vol. 175, 2002, pp.168-199.
7. Zhang, M.J., Lin, S. C., Yu, S. T., Chang, S. C. and Blankson, I., "Application of the Space-Time Conservation Element and Solution Element Method to the Ideal Magnetohydrodynamics Equations", AIAA Paper 2002-3888, 2002.
8. Zhang, M.J., Yu, S. T., Chang, S. C. and Blankson, I., "Direct Calculation of the Ideal MHD Equations by the CESE Method without Special Treatment of Constraint of $\nabla \cdot B = 0$", AIAA Paper 2003-0324, 2003.
9. Chang, S. C., Courant Number Insensitive CESE Method, AIAA Paper 2002-3890, 2002.
10. Chang, S. C., Wang, X.Y. and Chow, C.Y., "The Space-Time Conservation Element and Solution Element Method -- A New High-Resolution and Genuinely Multidimensional Paradigm for Solving Conservation Laws, The Two Dimensional Time Marching Schemes", NASA TM 209943, 1998.
11. Yee, H. C., Warming, R. F. and Harten, A., "Implicit Total Variation Diminishing (TVD) Scheme for Steady-state Calculations," AIAA Paper 83-1902, 1983.

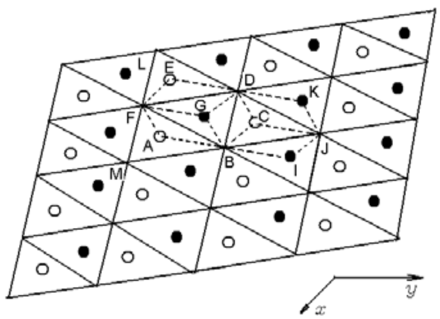

Fig. 1: Spatial computational domain with a triangular mesh. Circles (solid or hollow) are triangles' centroids.

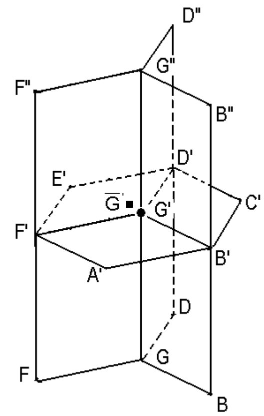

Fig. 4: Definition of Solution Element $SE(j,k,n)$ associated with point G' (j,k,n).

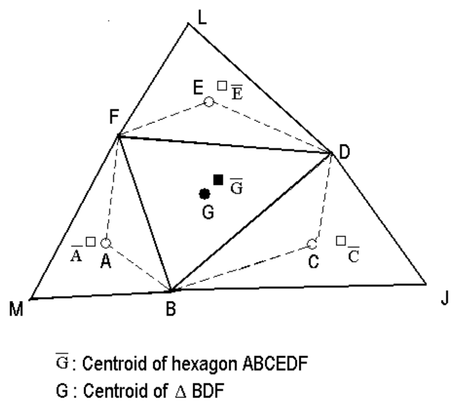

Fig. 2: Definition of the solution pooints.

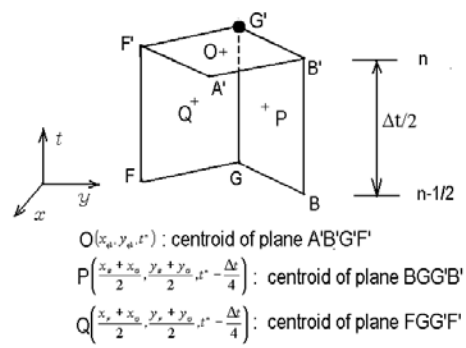

Fig. 5: Three surfaces of $SE(j,k,n)$ as a part of $CE_1(j,k,n)$.

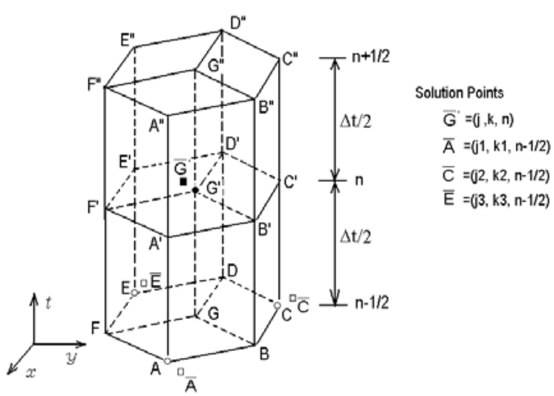

Fig. 3: Grid point arrangement in the space-time domain.

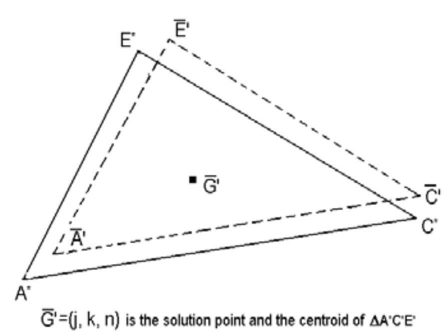

Fig. 6: Parallel translation of $\Delta\bar{A}'\bar{C}'\bar{E}'$ and $\Delta A^*C^*E^*$. Solution point $\bar{G}'$ is $\Delta A^*C^*E^*$'s centroid.

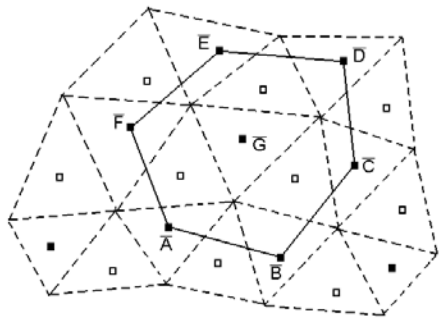

Fig. 7: The numerical domain of dependence in the CESE method.

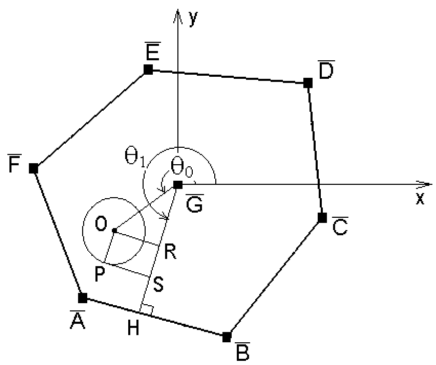

Fig. 8: Definition of the local CFL condition for the two-dimensional Euler equations.

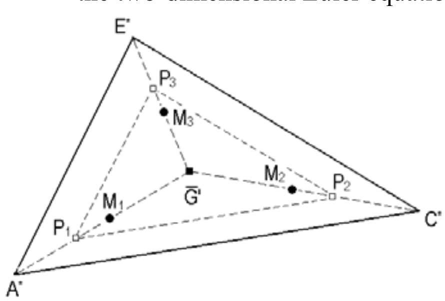

Fig. 9: Definition of points M_1, M_2, M_3, P_1, P_2 and P_3 for the CFL-insensitive schemes.

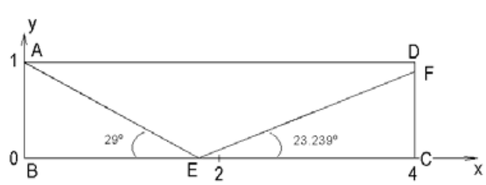

Fig. 10: The computational domain and the shock location of a steady state oblique shock problem [11].

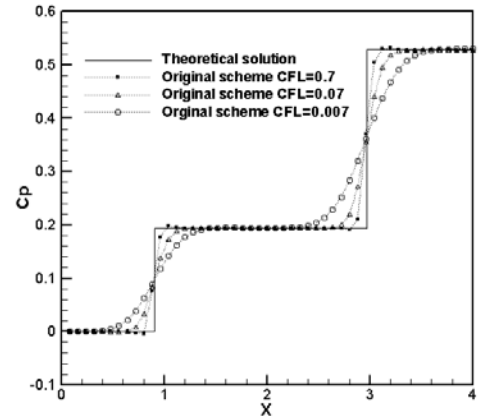

11a

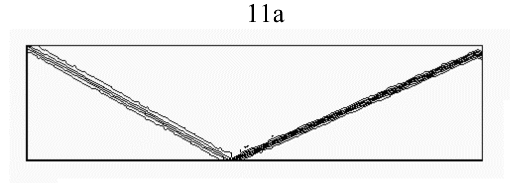

11b

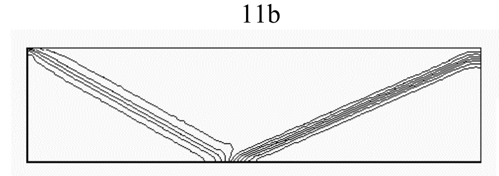

11c

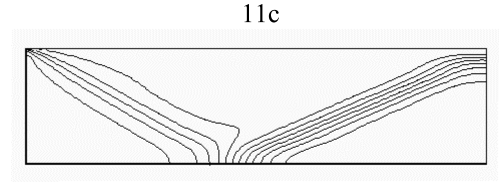

11d

Fig. 11: Solution of the oblique shock problem with uniform mesh by using the original CESE scheme. (a) Comparison between theoretical solution and numerical solutions at different CFL number along y =0.5. (b) Pressure contours at CFL=0.7. (c) Pressure contours at CFL=0.07. (d) Pressure contours at CFL=0.007.

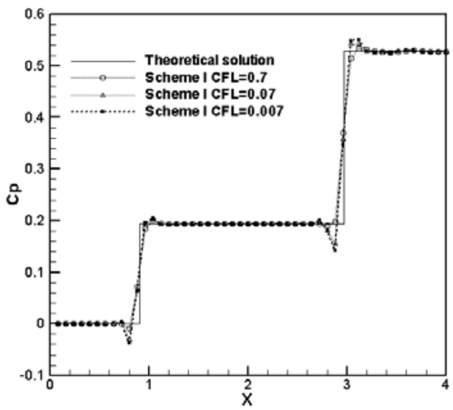

Fig. 12: Solution of the oblique shock problem with uniform mesh by using Scheme I. Comparison between theoretical solution and numerical solutions at different CFL number along line y = 0.5.

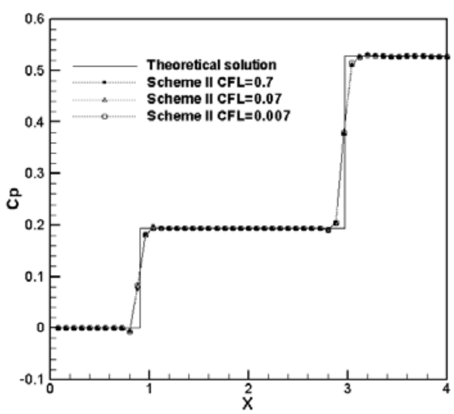

13a.

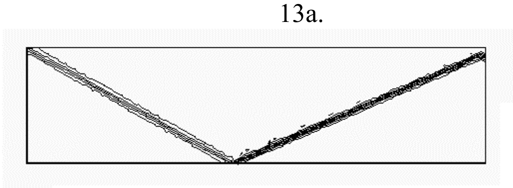

13b

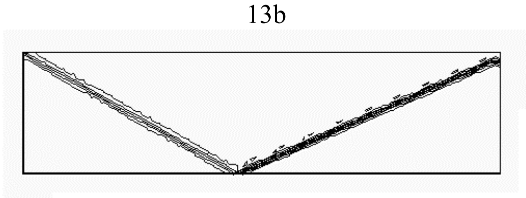

13c

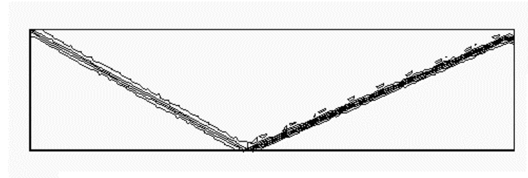

13d

Fig. 13: Solution of the oblique shock problem with uniform mesh by Scheme II. (a). Comparison between theoretical solution and numerical solutions at different CFL number along line y =0.5. (b) Pressure contours at CFL=0.7. (c) Pressure contours at CFL=0.07. (d) Pressure contours at CFL=0.007.

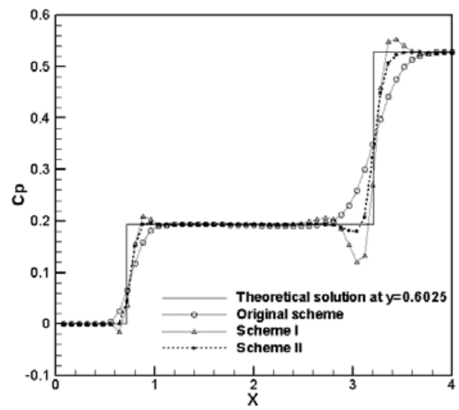

14a

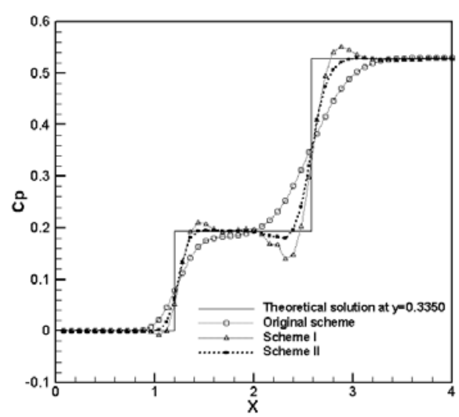

14b

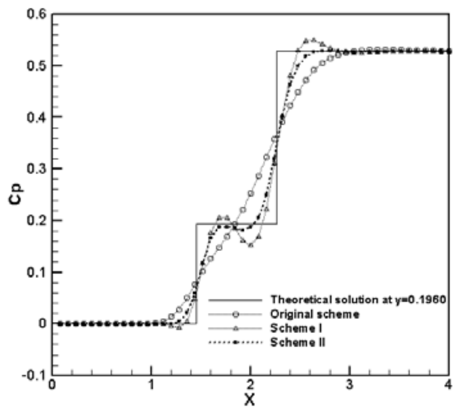

14c

Fig. 14: Solutions of the oblique shock problem by using different schemes on a non-uniform mesh. (a) Pressure coefficient distribution along line y = 0.6025. (b) Pressure coefficient distribution along line y = 0.3350. (c) Pressure coefficient distribution along line y = 0.1960.

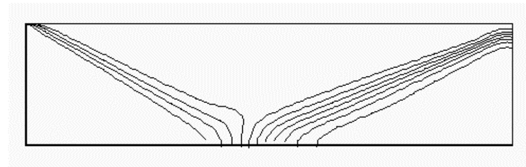

15a

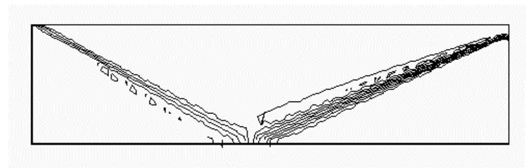

15b

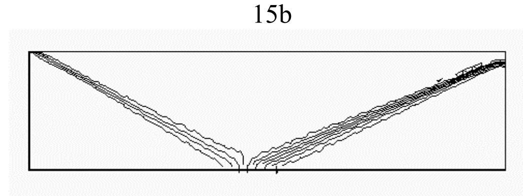

15c

Fig. 15: Pressure contours of the oblique shock problem by using different schemes on a non-uniform mesh. (a) The original CESE scheme. (b) Scheme I. (c) Scheme II.